*Research Article*

# Discrete Vortex Method Of Flow Around A Cylinder In A Channel Using Simple Grid System

**Wisnu Wardhana[1], Ede M. W.[2], Meitha Soetardjo[3]**
[1]Dept. of Ocean Engineering, Institut Teknologi Sepuluh Nopember
[2]Dept. of Marine Engineering, Institut Teknologi Sepuluh Nopember
[3]Indonesian Hydrodynamic Laboratory, BPPTSurabaya, Indonesia

**Article History**: Received:11 January 2021; Accepted: 27 February 2021; Published online: 5 April 2021

**ABSTRACT :** Modelling of unidirectional and oscillatory flows around a cylinder in a channel using a simple overlapping grid system are carried out. The importance of this cylinder-wall configuration is the effect of blockage which suppress the development of the vortex shedding The polar grid system of the cylinder is then overlapped with the rectangular grid system of the wall. The length of rectangular grid element is about the same as the length of the polar grid system in the cylinder surface. The use of such overlapping grid system is for reducing the CPU time, i.e. in calculating the vortex velocity since the CPU time in calculating the vortices velocity takes the longest time. This method is not only time efficient, but also gives a better distribution of surface vorticity as the scattered vortices around the body are now concentrated on grid point. In this study there is no vortex-to-vortex interaction, but instead it uses node-to-node interactions. Velocity calculation also uses this overlapping grid in which the new incremental shift position then summed up to get the total new vortices position. In this overlapping system the grid can be either off or on depend on process involved to get rid of the nodes not being used. The engineering applications of this topic is to simulate the loading pipeline placed in the channel such as in the heat exchanger or simulation of U-tube experiment or other system. The in-line and transverse force coefficients are found by integrating the pressure around the cylinder surface. The flow patterns are then can be obtained and presented. The comparison of the results with experimental evidence is presented and also the range of good results is discussed.

**KEYWORDS:**cylinder, channel, discrete vortex, polar grid, rectangular grid, overlapping grid

## 1. INTRODUCTION

Experimental visualization for flow around a cylinder with parallel slit placed inside a circular pipe has been carried out. Two different color dyes are employed to visualize the complex vortex formation mechanism behind the bluff bodies. The objective of this study is to explore the potential of cylinder with parallel slit as an improved vortex generator for various practical applications [1].

A numerical investigation of the flow past a circular cylinder center in a two-dimensional channel of varying width is presented. For low Reynolds numbers, the flow is steady. For higher Reynolds numbers, vortices begin to shed periodically from the cylinder. In general, the Strouhal frequency of the shedding vortices increases with blockage ratio. In addition, a two-dimensional instability of the periodic vortex shedding is found, both empirically and by means of a Floquet stability analysis [2].

The experiment in the Reynolds number range of 10 to 360 for a blockage ratio (ratio of the cylinder diameter to the channel height) of 0.2 have been done. This is to investigate the confinement effect due to the channel's stationary walls on the force coefficients and the associated Strouhal numbers. The results suggest a transition from a shedding flow regime between $Re^{¼}=180$ and $Re^{¼}=210$. A discontinuity in the variation of the Strouhal number *St*, and of the base pressure coefficient *Cp*, with *Re* was also observed [3].

Using a variety of flow-visualization techniques, the flow behind a circular cylinder has been studied. Using time-exposure photography of the motion of Aluminium particles, a sequence of instantaneous streamline patterns of the flow behind a cylinder has been obtained. These streamline patterns show that during the starting flow the cavity behind the cylinder is closed. However, once the vortex-shedding process begins, this so-called 'closed' cavity becomes open, and instantaneous 'alleyways' of fluid are formed which penetrate the cavity [4].

A flow past a cylinder immersed in a stream bounded by rigid walls is researched. This is subject to what is called the blockage effect. The overall effect is an increase in the free stream velocity, relative to the unbounded flow, which is related partly to the volume distribution of the body itself solid blockage, and partly to the displacement effect of the wake blockage [5].

The vortex shedding past a circular cylinder in a two-dimensional channel of varying height is presented in the term of Strouhal number using FLUENT 6.3. The computational grid structure is generated. In this analysis, the result is carried out with blockage ratio b=80, 0.83, 0.85, 0.88 and Reynolds number range from 50 to 300.

Proposed by [6], that the Drag Coefficient *Cd* in an unbounded stream is related to the drag $C_{dw}$ in a wind tunnel by

$$C_d = C_{dw}(1-\frac{\eta t}{h})^2 \quad (1)$$

where$t$ is the thickness of the bluff body, $h$ is the tunnel height, $\eta$ is an empirical factor which is found experimentally.

A theory for the blockage of the flow past a bluff body in a closed wind tunnel involving an approximate relation describing the momentum balance in the flow outside the wake is developed. As a results of the experiments, the correction formula is [7] :

$$\frac{\Delta P}{P} = \varepsilon C_d \frac{s}{c} \quad (2)$$

where$\Delta P$ is the effective increase in dynamic pressure due to the blockage constraint, and $\varepsilon$ is a blockage factor dependent on the magnitude of the base pressure coefficient. The factor $\varepsilon$ is shown to range between 5 for axis-symmetric flow to $\frac{5}{2}$ for two dimensional flow. In addition, $s$ is the area on which the profile drag coefficient $C_d$ is based, and $c$ is the cross-sectional area of the tunnel.

In the experiment carried out at the Imperial College London, used a correction for the blockage effect based on a function of the blockage ratio taken as the frontal area of the model to the cross section of the wind tunnel working station, which varied between 5% to 10% [8].

The formula used was as follow,

$$C_d^{corrected} = \frac{C_d^{measured}}{(1+\epsilon)^2} = (1-2\epsilon)C_d^{measured} \quad (3)$$

where $\epsilon = \frac{A}{2A_T} C_d^{\text{measured}}$ measured, $A$ is the reference frontal area of the model and $A_T$is the cross sectional area of the wind tunnel. The presence of walls close to a cylinder in a flow induces a significant effect on the cylinder and the flow characteristics.

A flow with blockage using a discrete vortex method in which the convection velocities were computed using a vortex-in cell method involving the solution of the Poisson equation. Diffusion was simulated by imposing random walks on each vortex in two orthogonal directions in a polar coordinate grid system. To model the boundaries, they used an overlapping system of rectangular and polar meshes. The outer mesh and the intermediate mesh were rectangular and the inner mesh was polar. Constant stream function values were imposed on the upper and lower boundaries [9].

Another approach are proposed in which the wall boundary condition of parallel flow may be obtained by reflection and modelling the flow as two interlaced cascades in which the pitch, the distance between two image bodies both above the upper wall and below the lower wall, is equal to the wall distance. Since the solution is the same for all wall reflections (but inverted), the Martensen equation may be applied with relatively simple modifications to the code. However, the approach has some limitations when the vortex-in-cell scheme is implemented in relation to calculating the vortex velocity. This is due to the fact that the node-to-node interaction is used instead of the vortex to vortex interaction. The difficulty will arise when the node points are located outside the fluid domain. This could happen since the node points can lie outside the two walls even though a point vortex is still located inside [10].

The numerical results [9], show that blockage corrections based on steady flow condition where a blockage ratio $D$ (the ratio of the distance between walls $G$ to cylinder di-ameter $D$) of 14 would give an effective increase in the free stream velocity of about 4% at aReynolds number of $10^4$. It would also cause an increase in the drag of about 8 per cent. At Reynolds number of 100 with a blockage ratio of 16, the mean drag increases as much as 2.5%. More significant increases in the mean drag exist for blockage ratios less than 8. At blockage ratios of 8,4, and 2, the mean drag increases as much as 10,43 and 210% respectively. The effect of the blockage on the Strouhal number shows a quite different trend. Increasing the blockage (reducing the blockage ratio) is seen to increase the Strouhal number down to a blockage ratio of about 4 %, while a blockage ratio of 2 has a lower Strouhal number than a blockage ratio of 4.

## 2. METHODOLOGY.

In the present study, the complex potential used comprises the contributions from the free stream velocity $u_\infty$, the cylinder surface vorticity $\gamma_n$, the wall surface sources $\sigma_\omega$ and the shed vortices $\Gamma_v$as follows,

$$\omega(z) = u_\infty e^{-i\alpha\infty_z} + \frac{i}{2\pi}\sum_{e=1}^{Ne}\gamma_e\, dS_e \ln(z-z_e) + \frac{1}{2\pi}\sum_{g=1}^{M_w}\sum_{\omega=1}^{N_\omega^\theta}\sigma_\omega^\theta\, dS_\omega^g \ln(z-z_\omega^g) + \frac{i}{2\pi}\sum_{v=1}^{N_v}\Gamma_v \ln(z-z_e) \quad (4)$$

The strength of a vortex $\gamma_n$and a source $\sigma_\omega^g$at element $\omega$ of the wall $g$ in this equation can be calculated by satisfying the Dirichlet boundary condition of zero tangential velocity on the cylinder surface and the Neumann boundary condition of zero normal velocity along the wall. $M_\omega$shows the number of walls for the case to be analyzed. $M_\omega$equal to two is for cylinders in channel.

The size of the rectangular grid segment is made equal to the size of the wall element. The velocity of a vortex can now be calculated through the use of the polar and the rectangular grid nodes. The addition contribution from the wall sources is implemented using the rectangular grid nodes. This implies that a bilinear interpolation and re-interpolation in polar and rectangular coordinates is needed to distribute and redistribute the vortex strength and velocity onto two grid node systems as explained in detail in the following sections.

The force coefficients can then be calculated by integrating the pressure distribution from the stagnation point to around the cylinder. The strategy of calculation in this study is shown in the flow chart in Figure 1.

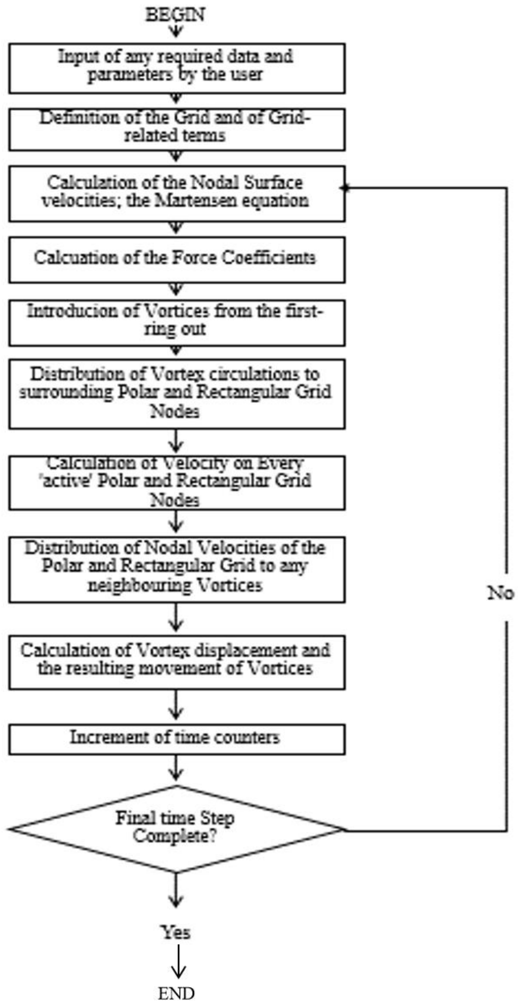

Figure 1.The flow chart of the numerical method

Problem using a discrete vortex model are analysed [11-13]. Their model contains an approximation as an infinite number of image vortices must be introduced in order to sat-isfy the non-permeability condition on the cylinder surface and on the plane boundary.

However, in the numerical calculations a finite number of images of about 9 is found to be sufficient because, as image vortices of equal and opposite strengths approach each other, a complete cancellation of the vortex pair results. Similar approximation to model the flow around two cylinders arranged normal to the free stream also used [14]. He claimed an accuracy of the zero normal velocity condition as small as $10^{-6}$ is achieved by using the same number of images as mentioned above.

Another method, which has been adopted in this study, is the distribution of source elements along the walls. Using an equation similar to equation (5) below, the Neumann boundary condition along the wall and the Dirichlet boundary condition along the cylin-der circumference can be satisfied simultaneously.

The complex potential equation (5) becomes :

$$\omega(z) = u_\infty e^{-i\alpha\infty_z} + \frac{i}{2\pi}\sum_{e=1}^{Ne}\gamma_e\, dS_e \ln(z-z_e) + \frac{1}{2\pi}\sum_{\omega=1}^{N_\omega^1}\sigma_\omega^1\, dS_\omega^1 \ln(z-z_\omega^1) + \frac{i}{2\pi}\sum_{v=1}^{N_v}\Gamma_v \ln(z-z_e) \quad (5)$$

in which $N_\omega^1$, shows the number of element of the walls.

**3. BASIC FORMULATION**

As there are two different boundary conditions imposed on the circumference of the cylinders and on the walls. The Martensen equation should be further modified and sep-arated into two expressions to take into account the influence of the wall as follow,

$$-\frac{1}{2}\gamma_m + \oint_e k_{mn}\,\gamma_n dS_n + \oint_e k_{mv}\,\sigma_\omega dS_\omega + \vec{u}_\infty.\vec{d}S_m + \sum_v^{N_v} l_{mv}\Gamma_v = 0 \quad (6)$$

and

$$\frac{1}{2}\sigma_e + \oint_e k'_{vn}\,\gamma_n dS_n + \oint_{c'} k'_{v\omega}\,\sigma_\omega dS_\omega + \vec{u}_\infty.\vec{d}S_e^n + \sum_v^{N_v} l_{cv}\Gamma_v = 0 \quad (7)$$

In which $k'_{vn}, k'_{v\omega}$and $k_{m\omega}$are the kernels of the integrals which are described later, $\sigma_\omega$is the strength of the wall source at point $\omega$. $\vec{d}S_m$ the tangential direction vector of the cylinder element in while $\vec{d}S_e^n$is the normal direction vector of the wall element *v*. This integration is taken along a closed curve joining the top wall from $-\infty$to $\infty$the circumference of the cylinders and the bottom wall from $-\infty$to $\infty$as shown in Figure 2.

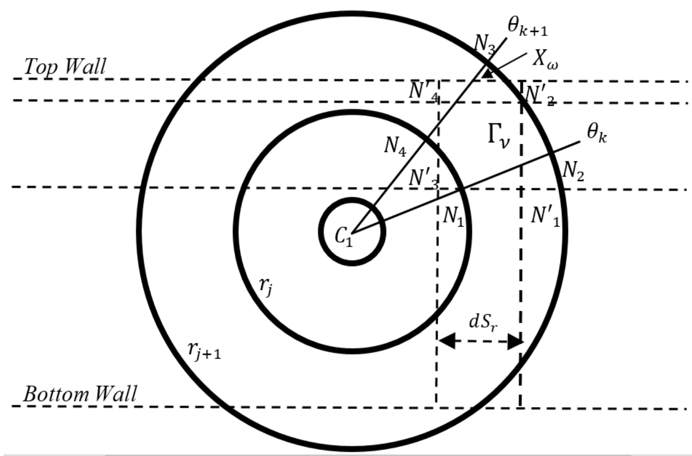


Figure 2.The overlapping grid system

Due to the nature of the kernel functions above, which are asymptotically equal to zero as the distance approaches infinity, the integration reduces to the integrals around the cylinder's surface and the two walls only.

The Dirichlet boundary condition of zero tangential velocity on the circumference of the cylinders implied in equation and the Neumann boundary condition of zero normal velocity along the walls implied in equation (5) are solved simultaneously.

The wall boundary condition can be specified in terms of the velocity potential as,

$$\frac{\partial\phi}{\partial n} = 0 \quad (8)$$

As the source strengths far distant from the cylinders are relatively small, their contribution is neglected beyond a cut-off at a certain finite distance from the cylinders, which produces a finite number of wall elements $N_\omega$ as as follows,

$$\sum_{n=1}^{N_e} k_{mn}\gamma_n dS_n + \sum_{h=1}^{M_\omega}\sum_{\omega=1}^{N_\omega^h} k_{m\omega}^h\sigma_\omega^h dS_\omega^h + \Re\left(u_\infty e^{-i(\alpha_\infty-\beta_m)}\right) + \sum_{v=1}^{N_v} l_{mv}\Gamma_v = 0 \quad (9)$$

to satisfy the Dirichlet boundary condition at element m of the cylinder circumference and

$$\sum_{n=1}^{N_e} k'^{g}_{vn}\gamma_n dS_n + \sum_{h=1}^{M_\omega} \sum_{\omega=1}^{N_\omega^h} k'^{gh}_{v\omega}\sigma_\omega^h dS_\omega^h + \Re\left(u_\infty e^{-i(\alpha_\infty-\beta_v^g)}\right) + \sum_{\nu=1}^{N_\nu} l'^{g}_{v\nu}\Gamma_\nu = 0 \tag{10}$$

to satisfy the Neumann boundary condition at element $v$ of the wall $g$. To find the unknown value of the vortex strength $\gamma_n$and the source strength $\sigma_v$ these equations can now be expressed in the matrix form as follows,

$$\begin{pmatrix} K_{mn} & K_{mv}^1 & K'^2_{m\omega} \\ K_{vn}^1 & K'^1_{v_1v_2} & K_{v\omega}^{12} \\ K'^2_{wn} & K'^2_{wv} & K'^{22}_{w_1\omega_2} \end{pmatrix}\begin{pmatrix} \gamma_n \\ \sigma_v^1 \\ \sigma_\omega^2 \end{pmatrix} = \begin{pmatrix} RHS \\ RHS^1 \\ RHS^2 \end{pmatrix} \tag{11}$$

where the components inside the matrix are all submatrices with $M_\omega$signifying the bottom and top wall.

The coupling coefficients representing the induced velocity at pivoting point *m* or *n* of the cylinder and at pivoting point *v* or w along the wall are then given by :

$$\begin{aligned} k_{mn} &= \Re\left(\frac{i\gamma_n}{2\pi}\frac{\Delta S_n e^{i\beta m}}{z_m - z_n}\right) \\ k_{m\omega} &= \Re\left(\frac{\sigma_\omega}{2\pi}\frac{\Delta S_\omega e^{i\beta m}}{z_m - z_\omega}\right) \\ k'_{vn} &= -\Im\left(\frac{i\gamma_n}{2\pi}\frac{\Delta S_n}{z_v - z_n}\right) \\ k'_{v\omega} &= -\Im\left(\frac{\sigma_\omega}{2\pi}\frac{\Delta S_\omega}{z_v - z_\omega}\right) \end{aligned} \tag{12}$$

There are two components inside the two $RHS^1$and $RHS^2$ blocks which contain the contribution of the free stream and the shed vortices as indicated in equation (9) and (10) above. The coupling coefficients $l_{mv}$and $l'_{wv}$, are similar to $k_{mn}$and $k'_{vn}$but with the value of $\Gamma_\nu$replaced by $\gamma_n\,\Delta S_n$.

Upon definition of all components inside the matrix equation (12) above, the unknown vortex and source strength $\gamma_n$and $\sigma_v$can be calculated through

$$[\gamma_n, \sigma_n] = [K_{mn}]^{-1}[RHS] \tag{13}$$

where $K_{mn}$is the left hand side matrix in that equation.

## 4. INTRODUCTION OF VORTICES IN THE FLOW

In this simple model in the present study, only the 'blockage' effect is considered and all the effects of the boundary layer interaction between cylinder and wall are ignored although Reynolds number effects are implicit in the choice of various model parameters such as the element lengths and grid dimensions. These have been largely specified on the basis of previous work and sensitivity studies [15,16].

## 5. DISTRIBUTION OF CIRCULATION TO THE GRID

This means that the strength of a vortex is distributed in its own surrounding polar grid nodes and the rectangular grid nodes. A vortex shed from other cylinders is also distributed in the same manner and stored in a different array. The polar grid nodes are used to evaluate the interaction among vortices shed from the same body while the rectangular grid nodes are used to evaluate the influence from vortices shed from the other cylinders.

It can be seen from Figure 2 that the use of polar grid elements close to the wall could create a situation where an active polar grid node is situated outside the fluid domain between the walls even though the vortex it represents, is still inside. This active node is then treated as usual, bearing in mind that the active nodes only represent a redistribution of vortices in the flow and also that there is no direct interaction between the polar grid nodes and the wall elements.

## 6. CALCULATION OF VELOCITY

The complex velocity at a point $z = x + iy$in the flow field is simply derivative as follows,

$$\frac{dw(z)}{dz} = u - iv = u_\infty e^{-i\alpha_\infty} + \frac{i}{2\pi}\sum_{n=1}^{N_e}\frac{\gamma_n dS_n}{z - z_n} + \frac{1}{2\pi}\sum_{h=1}^{M_w}\sum_{w=1}^{N_w^h}\frac{\sigma_w^h dS_w^h}{z - z_w^h} + \frac{i}{2\pi}\sum_{\nu=1}^{N_\nu}\frac{\Gamma_\nu}{z - z_\nu} \tag{14}$$

in which *u* and *v* are respectively the velocity components in *x* and *y* directions.

As the calculation of vortex velocity is done after the introduction of vortices into the flow, this equation has to be modified slightly by eliminating the second term of the RHS of equation (14) as the surface vorticity has already been released and absorbed in the shed vortices $N_v$ as follows,

$$\frac{d\omega(z)}{dz} = u - iv = u_\infty e^{-i\alpha\infty} + \frac{1}{2\pi}\sum_{h=1}^{M_\omega}\sum_{\omega=1}^{N_\omega^h}\frac{\sigma_\omega^h dS_\omega^h}{z-z_\omega^h} + \frac{i}{2\pi}\sum_{j,k}\frac{\Gamma_{j,k}}{z-z_{j,k}} \tag{15}$$

in which the $z_{j,k}$ shows the coordinate of the active grid nodes either in relation to the polar or the rectangular grid system. As shown in equation (15) above, the presence of walls which are modelled by source distributions leads to another factor contributing to the calculation of vortex velocities.

This source contribution in the second term of the equation is carried out through the use of the overlapping rectangular grid system. The velocity of the active rectangular grid nodes due to the source distribution of the walls is then,

$$\bar{u}_\omega(z) = \frac{1}{2\pi}\sum_{h=1}^{M_\omega}\sum_{\omega=1}^{N_\omega^h}\frac{\sigma_\omega^h dS_\omega^h}{z-z_\omega^h} \tag{16}$$

where $N_\omega^h$ is the total number of element at wall $h$.

The velocity of a vortex $v$ shed from the cylinder due to the wall is then found through the use of the bi-linear interpolation,

$$u_\omega(z_v) = Q_1(v)u_\omega(N_1) + Q_2(v)u_\omega(N_2) + Q_3(v)u_\omega(N_3) + Q_4(v)u_\omega(N_4) \tag{17}$$

This velocity should be added to the vortex velocity due to vortices shed from cylinder surfaces. Hence,

$$u(z_v) = u_v(z_v) + u_{p\omega}(z_v) + u_{r\omega}(z_v) \tag{18}$$

where, $u_v(z_v)$ is the vortex velocity due to other vortices shed from the cylinder, $u_{p\omega}(z_v)$ is the vortex velocity due to the influence of the walls and $u_{r\omega}(z_v)$ is the vortex velocity due to diffusion random walk.

## 7. METHOD OF ENHANCEMENTS

The influence of the member of sources modelling the wall on the fluid velocity just outside the cylinder surface element closest to the wall are shown choosing the case of the wall proximity for the test. It can be seen that the rate of change of the cylinder surface vorticity strength $\gamma_k$ to the wall extension $\frac{\partial\gamma_k}{\partial z_\omega}$ is less than 0.01, when the distance of the end wall elements to the cylinder center is not less than 3D.

This value is then used to determine the wall length after shedding vortices. The wall end points can be determined by measuring this distance from the extreme position of a vortex, see Figure 3 below.

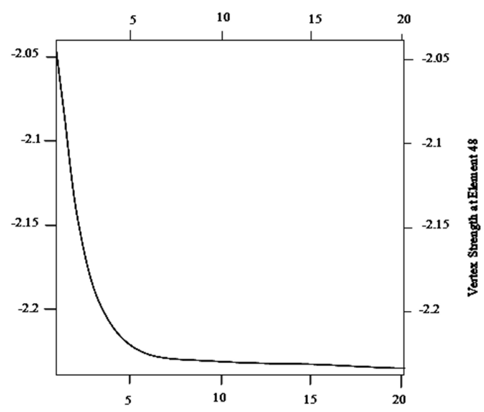


Figure 3.Effect of the wall length to the cylinder

## 8. RESULT AND DISCUSSION

### a) Uni-directional Flow

The simulation is tested using one bottom wall only at G/D=1.2 and Re=2x$10^4$ by comparing with the available experiment data shown in Figure 4. It is shown that the result of that using single wall is similar to experiment in which the separation flow close to the wall is shifted to around 125 degrees while the one on the top is shifted to around 135 degrees.

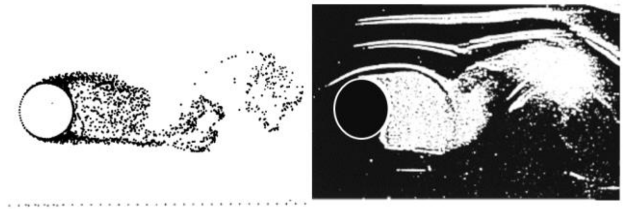

Figure 4.Comparison of the flow pattern numerical vs lab. Experiment at G/D= 1.2 and Re= $2x10^4$

The shear layer emanating from the lower half of the cylinder seems to stretch longer the upper one even though no force asymmetry was implemented. The formation region also seems to be slightly longer than that of isolated cylinder by about 5%. This is due to the fact that the close presence of the wall creates an asymmetric velocity field around the circumference of the cylinder in which the velocity is higher below the cylinder. The asymmetric velocity field around the cylinder also promotes the roll-up of the vortices earlier than that of the isolated cylinder. See Figure 4 above.

This prove is chosen because the author is not aware that there is a laboratory photographs for the flow in a channel.The results produced from some flow in a channel are presented with both flow visualizations and graphs showing the accompanying force coefficients. For the non-dimensional times of $\widehat{t}$ =1 and 5, the gap *C* is defined as the distance between the two walls, at a gap-diameter ratio G/D = 3 and Re = 100, the early structure of the wake behind the cylinder is shown in Figure 5. The separation points show a little shift compared with an isolated cylinder for which they occur at, about 100° measured from the positive X-axis. This figure also shows that, by imposing the same asymmetric shift,the blockage effect induces a tendency to delay the roll up of the vortices behind the cylinder.

Due to the higher velocity at and around the separation points,the length and width of the formation region arc longer and narrower respectively. Compared with those of the isolated cylinder. As described [8], the shape and size of the formation region significantly influences the reactive force exerted on the cylinder and the wake pattern behind. Figure 5 shows the influence of the wall on the formation region at t =1 and t = 5.

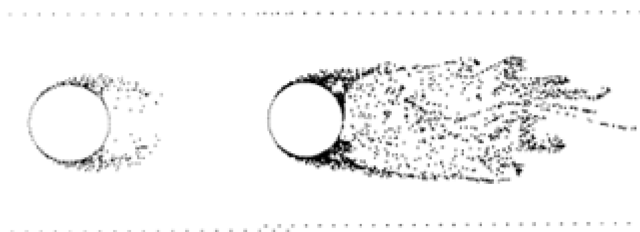

Figure 5.The flow pattern at $\widehat{t}=Ut/d$=1 and $\widehat{t}$=5

After the flow develops further as shown in Figure 5, regular vortex shedding occurs. It can be seen that, due to the presence of the walls, the wake is suppressed at a distance of about 4D behind the cylinder to form a Von Karman vortex street with the width equal to the wall distance. The value of Strouhal numbers is discernable at about 0.175, which is in fairy close agreement with the results of [9].

The figure also displays the force coefficients predicted for this flow plotted against the non-dimensional time. The drag coefficient is 2.4, which is slightly less than the result of previous research of 2.45 [9]. This result shows an increase of about 12% over that of the isolated cylinder with the same Reynolds number. It is a general trend that the higher the gap ratio D, the smaller the drag coefficient, until it reaches the value of the isolated cylinder.

The mean value of the lift coefficient, on the other hand, does not change from zero, even though it is shown that the average extreme values are slightly increased to around +/- 0.9. The rms lift is found to be 0.55 which is also close to the results of previous investigation [9]. It is particularly noticeable that the drag frequency is still around twice that of the lift, even though the 'noise' is more pronounced in this case, which seems that this blockage does not significantly change it from that of an isolated cylinder. This has to be the case while vortices are shed symmetrically from both sides of the cylinder.

Table 1.The CPU percentage of each algorithm section

| **Section Number** | **Purpose of Section** | **CPU Time (%)** |
|---|---|---|
| 1 | Input/output | 1.59 |
| 2 | Define Grid | 0.00 |
| 3 | Calculate Nodal Velocity | 74.37 |

| | | |
|---|---|---|
| 4 | Calculate Vortex Velocity | 1.75 |
| 5 | Vortex Displacement | 4.3 |
| 6 | Distribute Circulation | 1.2 |
| 7 | Calculate Surface Velocity | 16.75 |
| 8 | Calculate Forces | 0.04 |

The percentage of CPU time used in this algorithm during each section is presented in Table 1. The time taken for calculating the surface velocity has increased as much as 5 per cent compared with the isolated cylinder and this also contributes to the time needed for the matrix multiplication since the matrix size is now increased due to the presence of the wall sources. The influence of the rectangular element size, as described previously, shows a quite significant change in the percentage configuration especially for the time taken for calculating the nodal velocity which increases by around 6 %. All those CPU time percentages are taken at i= 90 when the flow has developed sufficiently to have a high number of the active polar nodes, active rectangular nodes and vortices.

Vortices with small strength compared to the others and those that move across the cylinder and the walls are all eliminated from the flow. This is conducted to maintain a more realistic flow pattern and to get a better reactive forces. The total strength of those vortices is then manipulated in such a way, to conserve the total circulation in the fluid domain.

The results for higher gap ratios *G/D* of 2,4,5,6, are presented in Figures 6, 7, 8, and 9. The general pattern to be observed from the results, not surprisingly, is that the higher the gap ratio the more the flow pattern and the force coefficients approach the values of the isolated cylinder.

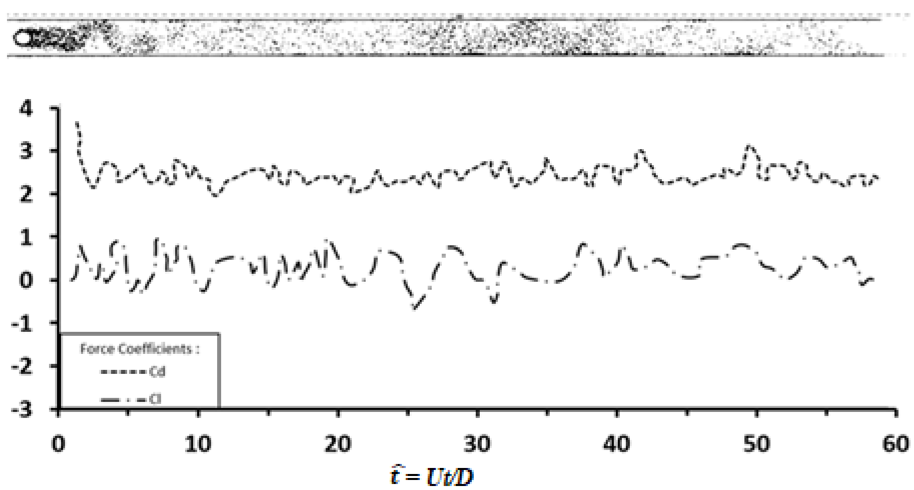


Figure 6. Flow pattern at $\hat{t}$ = 60 for G/D = 3 and Re = 100

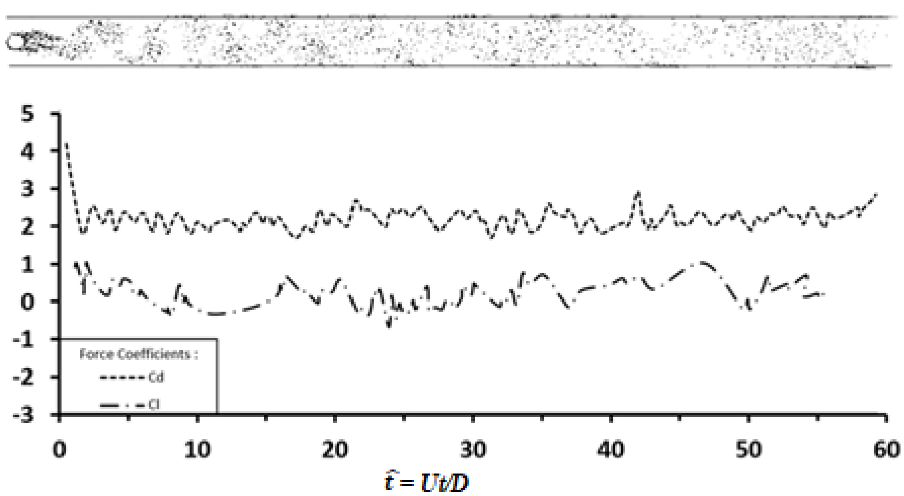


Figure 7. Flow pattern at $\hat{t}$ =60 for G/D = 4 and Re = 100

At a gap ratio of *G/D*=4 the drag coefficient is equal to 2.25, close to the results of [9]. While the extreme values of the lift coefficient are slightly increased to 0.7 with the rms lift value of around 0.39. There is no noticeable change in the value of the Strouhal number compared to the previous case. Due to the presence of the wall, the regular Von Karman vortex sheet behind the cylinder is suppressed at distance of about 6D as its width is constrained by the walls.

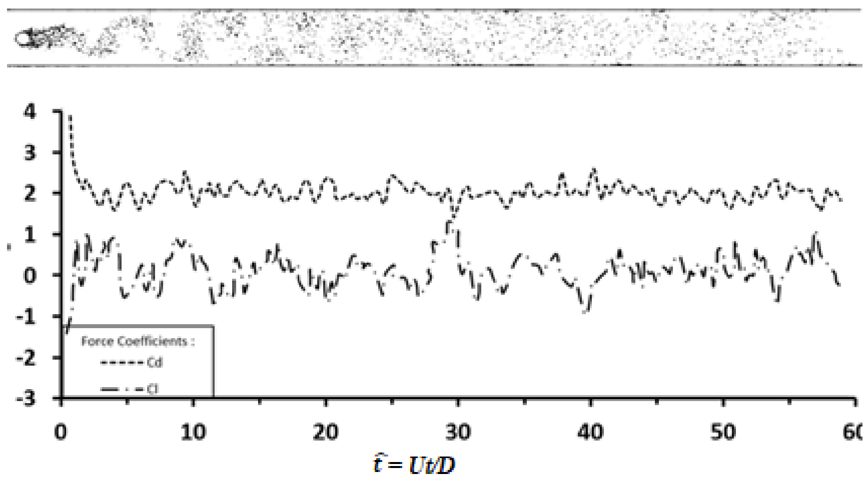


Figure 8. Flow Pattern at $\hat{t}$ = 60 for G/D = 5 and Re = 100

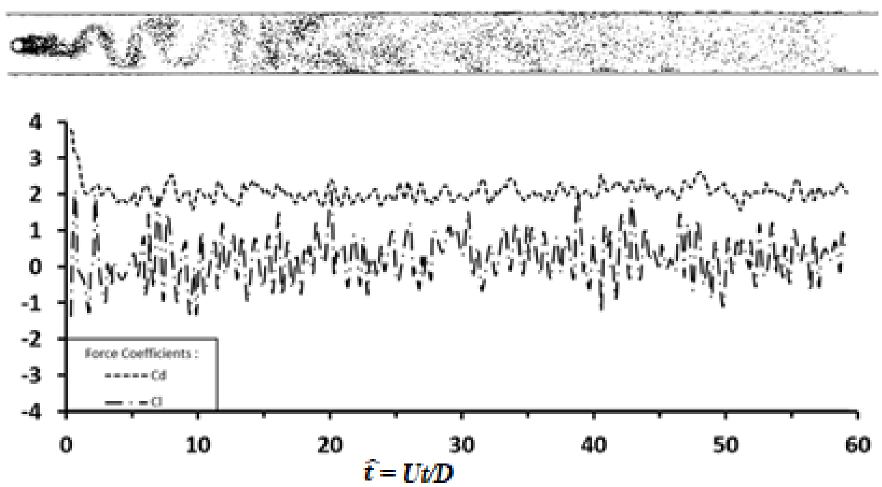


Figure 9. Flow pattern at $\hat{t}$ = 60 for G/D = 6 and Re = 100

A continuing decrease in the drag coefficient occurs when the gap ratio G/D = 5, its value being equal to around 2.15. The extreme value for the lift coefficient is slightly increased compared to the previous case with a rms value of around 0.41. The Strouhal number is still around 0.18. When D equals 6, the values of the drag coefficient is 1.9. These values are in good agreement with those found by the numerical approach by [9]. The lift coefficient approaches a value of 0.8 which is the same value as for the isolated cylinder. The Strouhal number also increases to around 0.2.

For a low gap ratio G/D = 2, a completely different trend is to be observed, in which the behavior of the vortices, due to the narrow gap between the wall and the cylinder, changes in the vicinity of the cylinder and along the wall, so as to increase the suppres-sion of the flow oscillation behind the cylinder. The drag coefficient could be raised to about 4.9, while that found in the present model is around 3 with the rms lift around 0.772.

The influence of Reynolds number at a certain gap ratio *G/D*=6 is also investigated using the model by varying the Reynolds number from 500 to 100000. The results for Re = 500, suggest that the drag is increased to around 1.6, which is about 10 % increase com-pared to that of the isolated cylinder. The extreme value of the lift coefficient is about 0.8 which is close to that of the isolated cylinder. As the Reynolds number is increased to around 1000, the drag coefficient is slightly reduced to 1.46. The extreme value of the lift coefficient is also reduced to around 1.75 and the Strouhal number is maintained around 0.2. The resolution of the picture is improved and it is seen clearly that the vortices approach the wall tangentially whenever they move close to it.

With the increase of the Reynolds number to 10000 and to 100000, the increase of the drag coefficient is in the range of 5 -10 % compared to the isolated cylinder. No difference in the value of the lift coefficient and the Strouhal number can be detected.

The results for a cylinder placed in a channel with *G/D*=2 to 6, Reynolds numbers of 100 and 100000 can then be summarized in the following table.

Table 2. Result for the flow around a cylinder in a channel at Reynolds number 100

| **Gap Ratio G/D** | **Drag Coefficient Cd** | **Lift Coefficient CL** |
|---|---|---|
| 2 | 3 | 0.05 |
| 3 | 2.4 | 0.05 |
| 4 | 2.25 | -0.04 |
| 5 | 2.15 | -0.01 |
| 6 | 1.9 | 0.04 |

Table 3. Result for the flow around a cylinder in a channel at gap ratio G/D = 6 at various *Re*

| **Reynolds Number Re** | **Drag Coefficient Cd** | **Lift Coefficient CL** |
|---|---|---|
| 100 | 1.9 | 0.05 |
| 500 | 1.6 | 0.05 |
| 1000 | 1.46 | -0.04 |
| 10000 | 1.2 | -0.01 |
| 100000 | 1.15 | 0.04 |

**b) Oscillatory Flow**

When a circular cylinder is subjected to oscillating flow as shown in figure below, the flow velocity oscillations result in variations of the drag and fluid inertia forces. Moreover, since vortex sheddingfrom the circular cylinder is also present, excitation transverse to the flow direction also occurs. The result is superposed (in-flow+transverse) bending vibration of the circular cylinder induced by the oscillating flow. A feature of the resulting vibration is that the in-line vibration component induced by the flow oscillations is much more dominant. Flow oscillations are normally characterized by a reduced velocity *Kc*, where $V_m$ is the amplitude of the oscillating flow velocity, and $f_{osc}$ the corresponding frequency of oscillation.

$$Kc = \frac{Vm}{fosc\ D}$$

The dimensionless quantity (Kc) is known as the Keulegan–Carpenter number [18]

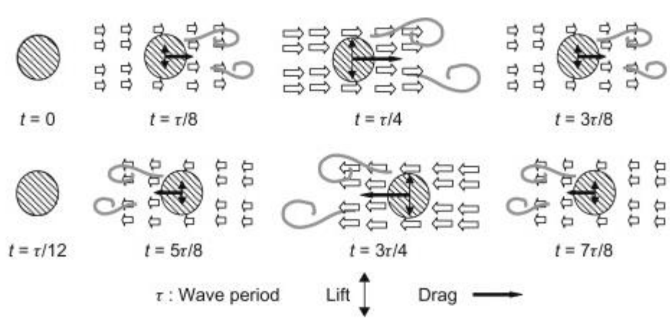


Figure 10,- Water flow around a Pipe-

As shown n the figure that due to oscillatory flow, the water flow to the right and left according to the the water flow as shown in the figure above. At a gap ratio *G/D* of 3, the present model was run at several values of the Keulegan-Carpenter number of 5, 10, 15, and 20 for Reynolds number 100000. The number of cylinder elements

*Ne*and the time step $\Delta t$ were chosen to be exactly the same as those in the previous chapter, namely 64 and 0.1 respectively. The vortices are also released from the first ring-out of the cylinder at a distance that varies as a function of the inverse of the square root of the ß value.

At Keulegan-Carpenter number of 5 the difference of the flow pattern at the early stages of the flow compared to that of the isolated cylinder as described in the previous section, is mainly that the blockage effect slightly narrows the wake downstream, as shown in Figure 10 for non-dimensional time $\hat{t}$ = 1 and 5 respectively. After the flow has developed further at $\hat{t}$ =60, it is seen that the wake is mostly concentrated close to the cylinder and spread along the wall. This is due to the fact that the velocity in the gap region is higher than the rest of the area, which can convect the vortices that fall in this region farther away than those that fall in the middle region between the walls. Also vortices in close proximity to the walls pair with their images in the wall and the two mutually convect each other along the wall.

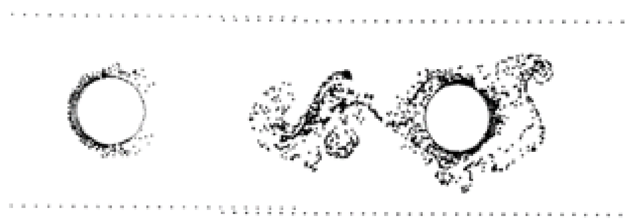

Figure 10. The Flow Pattern at, $\hat{t}$ =1 and 5. *G/D* = 3, and *Re* = 100000

Figure 11 shows that due to the blockage effect, the mean extreme value of the in-line force coefficient is slightly increased by about 6% compared to that of the isolated cylinder. In fact this value is closer to the experimental results of [14]. Due to the existence of the phase difference between the present and the experimental results, no improvement is obtained for the value of the drag and inertia coefficients which are 1.5 and 1.9 respectively.

At at higher Keulegan-Carpenter number of 10, as displayed in Figure 12, a similar trend occurred with an increase in the in-line force coefficient of about7%. Starting from the value of the Keulegan-Carpenter number and higher. As shown in Figures 13 and 14, this increase is accompanied by an improvement in the phase difference between the present results and the experimental results. The clear difference of the flow pattern compared to that of the isolated cylinder is that the wake around the cylinder is spread and bounded only between the two walls and this may cause a more pronounced influence of the shed vortices on the cylinder during the reversed flow and this will add to the influence of the wall itself.

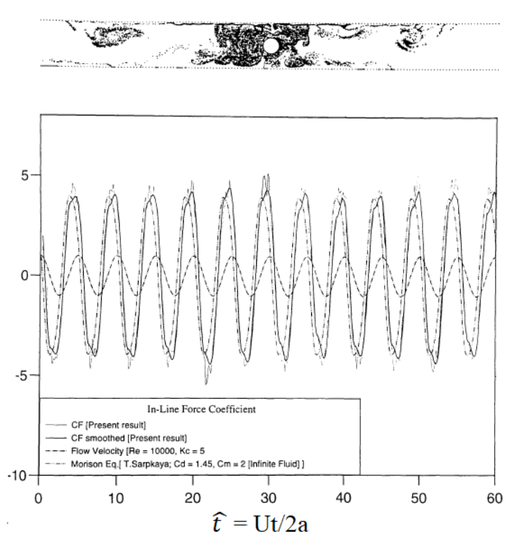


Figure 11. The Flow Pattern at $\hat{t}$ = 60, and the Force Coefficients for *G/D = 3, Kc = 5*, and *Re = 100000*

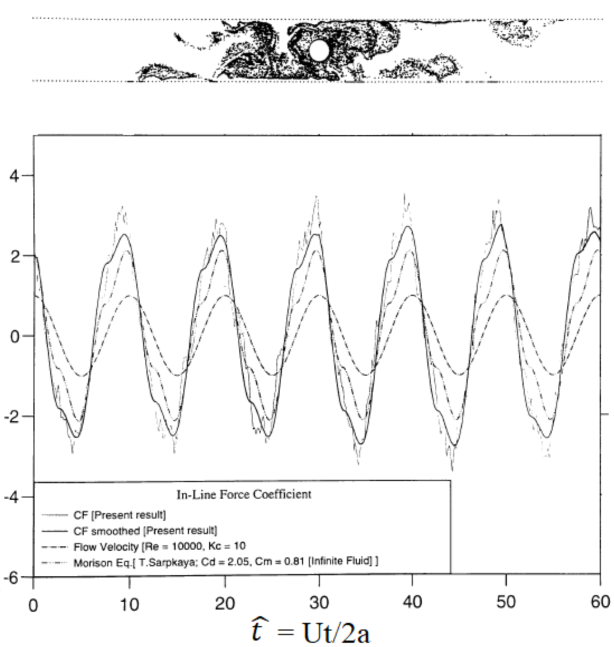


Figure 12. The Flow Pattern at $\hat{t}$ = 60, and the Force Coefficients for G/D = 3, Kc = 10, and *Re = 100000*

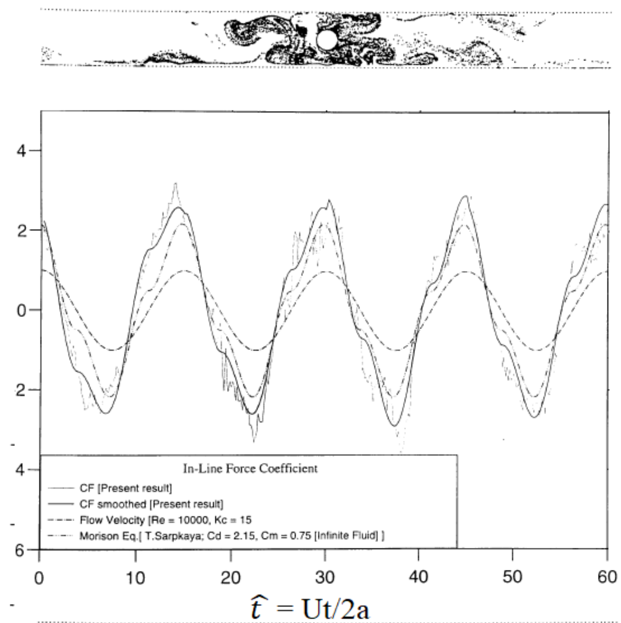


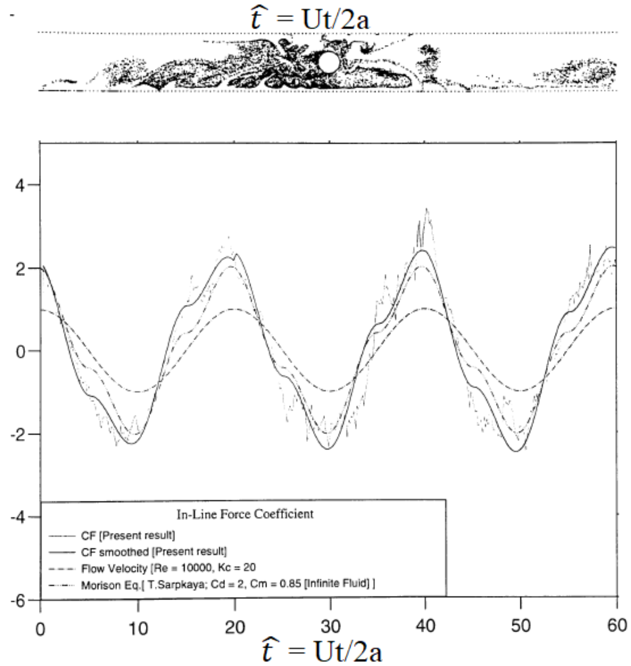


Figure 13. The Flow Pattern at $\hat{t}$ = 60, and the Force Coefficients for *G/D = 3, Kc = 15*, and *Re = 100000*

Figure 14. The Flow Pattern at $\hat{t}$ = 60, and the Force Coefficients for *G/D = 3, Kc = 25*, and *Re = 100000*

**9. CONCLUSSIONS**

Another extension of the discrete vortex model for investigating the flow around a single cylinder placed in a channel in unidirectional flow has been presented. The wall is modelled by a line source distribution of finite length. The interaction between the wall and the cylinder and its shed vortices has been computed through the use of two overlap-ping grids, the polar grid expanding from the cylinder and a uniform rectangular grid. In this model, the size of the wall source element is equal to the size of the polar grid segment in the cylinder surface. Two different kinds of boundary conditions are solved simultane-ously on the cylinder, with zero tangential velocity, and on the wall, with zero normal ve-locity. The influence of the vortices on the cylinder is computed using the polar grid node while that of the wall is computed using the rectangular grid. In other words, there is no direct calculation of the interaction between the wall and the active polar grid nodes. This grid strategy was chosen in an attempt to get a satisfactory interaction between the cylinder, shed vortices and the wall sources. In the case of a cylinder placed in a channel, the increase of the drag coefficient in unidirectional flow is in a good agreement with the available reference except when the channel width is small compared with the cylinder diameter.

**ACKNOWLEDGEMENTS**

The Author would like to thank Prof. Martin J. Downie for his patient supervision. Thanks also to Bilal Pradanahadi for typing this paper. The gratitude is also given to Diar and Frea M. Wardhana for their patient and help during the research**.**

**REFERENCES**

1. Ordia, L., Venugopal, A., Prabhu, S.V. (2017). Vortex Shedding Characteristics of a Cylinder with a Parallel Slit Placed in a Circular Pipe. Journal of Visualization 20(2), 263-275
2. Griffith, M. D., Leontini, J., Thompson, M.C., Hourigan, K. (2011). Vortex Shedding and Three-Dimensional Behavior of Flow Past a Cylinder Confined in a Channel. Journal of Fluids and Structures, 27, 855-860.
3. Kanaris, N., Grigoriadis, D., Kassinos, S. (2011). Three Dimensional Flow Around a Circular Cylinder Confined in a Plane Channel. Journal of Physics of Fluids, 23, 064106.
4. Perry, A. E., Chong, M. S., Lim, T.T. (2006). The Vortex-Shedding Process Behind Two-Dimensional Bluff Bodies. Journal of Fluid Mechanics, 116, 77-90.
5. Dhananjay Y., Srivastava, R., Lee, J. (2015). Numerical Simulation of Vortex Shedding Past a Single Cylinder Confined in a Channel. Journal of Fluid Mechanics, 1(1), 1-4.
6. Hermann Glauert. (1948). The Elements of Aerofoil and Airscrew Theory. Cambridge:Cambridge University Press.
7. Maskell, E.C. (1963).A theory of the Blockage Effects on Bluff Bodies and Stalled Wings in a Closed Wind Tunnel. Aeronautical Research Council: Reports and Memoranda No. 3400, Ministry of Aviation, UK.
8. Downie, M. J., Murray, B. A., Bettess, P. (1989).Calculation of the Force Coefficients of a Tubular Jacket Structural Member with an Appurtenance by the Discrete Vortex Method. Journal for Numerical Method in Engineering, 27, 153-167.
9. Stansby, P. K., &Slaouti, A. (1993). Simulation of Vortex Shedding Including Blockage by the Random-Vortex and Other Methods. International Journal for Numerical Methods in Fluid, 17, 1003-1013.
10. Spalart, P. R. (1984). Two Recent Extensions of the Vortex Methods. In Proceedings of 22nd Aerospace Sciences Meeting, Reno, USA.
11. Khan, Sher Afghan, et al. "Flow control with aero-spike behind bluff body." *International Journal of Mechanical and Production Engineering Research and Development* 8.3 (2018): 1001-1008.
12. Efthymiou, R.,&Narayanan, R. (1981). Wave Forces on Submarine Pipelines. Journal of Proceedings of Institution of Civil Engineering, 71(3), 773-787.
13. Efthymiou, R.,& Narayanan, R. (1982). Current Induced Forces on Submarine Pipelines, A Discrete Vortex Model. Journal of Proceedings of Institution of Civil Engineering, 73(1), 109-123.
14. Mandapudi, Snigdha, et al. "CFD simulation of flow past wing body junction: a 3-D approach." *International Journal of Mechanical and Production Engineering Research and Development* 7.4 (2017): 341-350.
15. Ali, H., & Narayanan, R. (1985). Hydrodynamic Forces on Cylinder above Plane Bed. In Proceedings of Fourth Int. Conf. on Offshore Mechanics and Arctic Engineering, Houston, USA.
16. Stansby, P.K. (1981). A Numerical Study of Vortex Shedding from One and Two Circular Cylinder. Journal of Aeronautical Quarterly, 32(1), 48-71.
17. Alizadeh, Asad, and Anas Abid Mattie. "Two-Dimensional Simulation To Investigate The Interaction Of Fluid-Structure Inside A Microchannel With Elastic And Rigid Boundary." *International Journal of Mechanical and Production Engineering Research and Development (IJMPERD) 9. 4, Aug 2019, 1151* 1156.
18. Downie, M.J. (1989). An Inviscid Model for the Fluid Forces Induced by Vortex Shedding from a Circular Cylinder (PhD Thesis). Royal Military College of Science, Shrivenham, UK.
19. Murray, B. A. (1992). Hydrodynamic Loading due to Appurtenances on Jacket Structures(PhD Thesis). Newcastle University, Newcastle upon Tyne, UK.
20. Umesh, K., V. Pravin, and K. Rajagopal. "An approach (performance score) for experimental analysis of exhaust manifold of multi-cylinder SI engine to determine optimum geometry for recreational and commercial vehicles." *International Journal of Automobile Engineering Research and Development (IJAuERD)* 4 (2014): 2277-4785.
21. Turgut Sarpkaya&Michael Isaacson. (1981). Mechanics of Wave Forces on Offshore Structure. Van Nostrand Reinhold and Company.
22. Tomomichi Nakamura (2013). Fow Induced Vibration, Elsevier.

23. Muthukumar, S., ESWARI PREM, and S. Suresh Kumar. "Mixed convective heat transfer in a rectangular nanofluid filled cavity with inclined magnetic field." *International Journal of Mechanical and Production Engineering Research and Development, 9 (5), 1179–1190. https://doi. org/10.24247/ijmperdoct2019104* (2019).
24. SAIKUMAR, KARTHIK. "DESIGN AND DEVELOPMENT OF PERMANENT MAGNET SYNCHRONOUS GENERATOR (PMSG) BASED ON SVPWM TECHNIQUES USING WIND ENERGY SYSTEM." International Journal of Electrical and Electronics Engineering Research (IJEEER) 6, 2, Apr 2016, 1-12